Annales
Geophysicae

Observed and predicted characteristics of equatorial F1 layer during solar minimum

C.-C. Lee

General Education Center, Chien Hsin University of Science and Technology, No.229, Jianxing Rd., Zhongli City, Taoyuan County 320, Taiwan

Correspondence to: C.-C. Lee (cclee@uch.edu.tw)

Abstract. This study aims to assess the predictability of IRI-2012 on the equatorial F1 layer during solar minimum. The observed characteristics of F1 layer by the Jicamarca digisonde are compared with the model outputs. The results show that the time range for F1-layer appearance of observation is longer than that of IRI-2012, by at least 1 h in the early morning and later afternoon. In IRI-2012, there are three options for the occurrence probability of F1 layer: IRI-95, Scotto-97 no L, and Scotto-97 with L options. The first option predicts the probability well, but the last two underestimate the probability. The peak density of F1 layer (NmF1) of observation is very close to that of IRI-2012. For the F1 peak height (hmF1), the modeled values are smaller than the observed ones. The observed seasonal variation of hmF1 is not found in the modeled results. Nevertheless, the observed diurnal variation of hmF1 is similar to the modeled results with the B0 choices of Bil-2000 and ABT-2009. Regarding the shape parameter, the values of D1 (the shape parameter of F1 layer in observation) are much greater than the values of C1 (the shape parameter of F1 layer in IRI-2012). The D1 values are 3–6 times the C1 values. The diurnal variation of D1 is similar to that of C1, but the seasonal variation of D1 is not.

Keywords. Ionosphere (equatorial ionosphere; modeling and forecasting)

1 Introduction

In 1969, the Committee on Space Research (COSPAR) and the International Union of Radio Science (URSI) initiated the International Reference Ionosphere (IRI). IRI is an empirical standard model of the ionosphere, based on all worldwide available data from ground-based and satellite observations (e.g., Bilitza, 1990). Since the late 1960s, IRI has been continuously improved with newer data and better model techniques. These processes have resulted in several major milestone editions of the model, including the IRI-78 (Rawer et al., 1978), IRI-85 (Bilitza, 1986), IRI-1990 (Bilitza, 1990), IRI-2001 (Bilitza, 2001), and IRI-2007 (Bilitza and Reinisch, 2008). The latest edition of IRI model is the IRI-2012 (http://iri.gsfc.nasa.gov/).

In order to evaluate the predictability of IRI, the modeled outputs are usually compared with measured ionospheric variables. In the equatorial ionosphere, there were many studies applying ionosonde and digisonde data to validate the F2-layer parameters of IRI model (Adeniyi and Adimula, 1995; Adeniyi and Radicella, 1998a, b; Reinisch and Huang, 1998; Adeniyi et al., 2003; Obrou et al., 2003; Abdu et al., 2004; Batista and Abdu, 2004; Lee and Reinisch, 2006, 2012; Lee et al., 2008). The F2-layer parameters are the F2-layer peak electron density (NmF2), its height (hmF2), and the bottom-side profile parameters (B0 and B1). In these previous studies, the comparisons between the observed and predicted results were conducted in different longitudinal sectors and in different solar epochs. Unlike the study of F2 layer, however, there is less work on the equatorial F1 layer than on the equatorial F2 layer. Adeniyi (1996) might be the only study, which compared the observed F1-layer peak density (NmF1) and height (hmF1) with the IRI modeled outputs at Ibadan, Nigeria (7.4° N, 3.9° E; dip latitude: 6.3° S).

As mentioned above, the studies for the equatorial F1 layer are very few. Furthermore, it is important that IRI provides well-established ionospheric profiles for the ionospheric scientists. Accordingly, a validation for all F1-layer
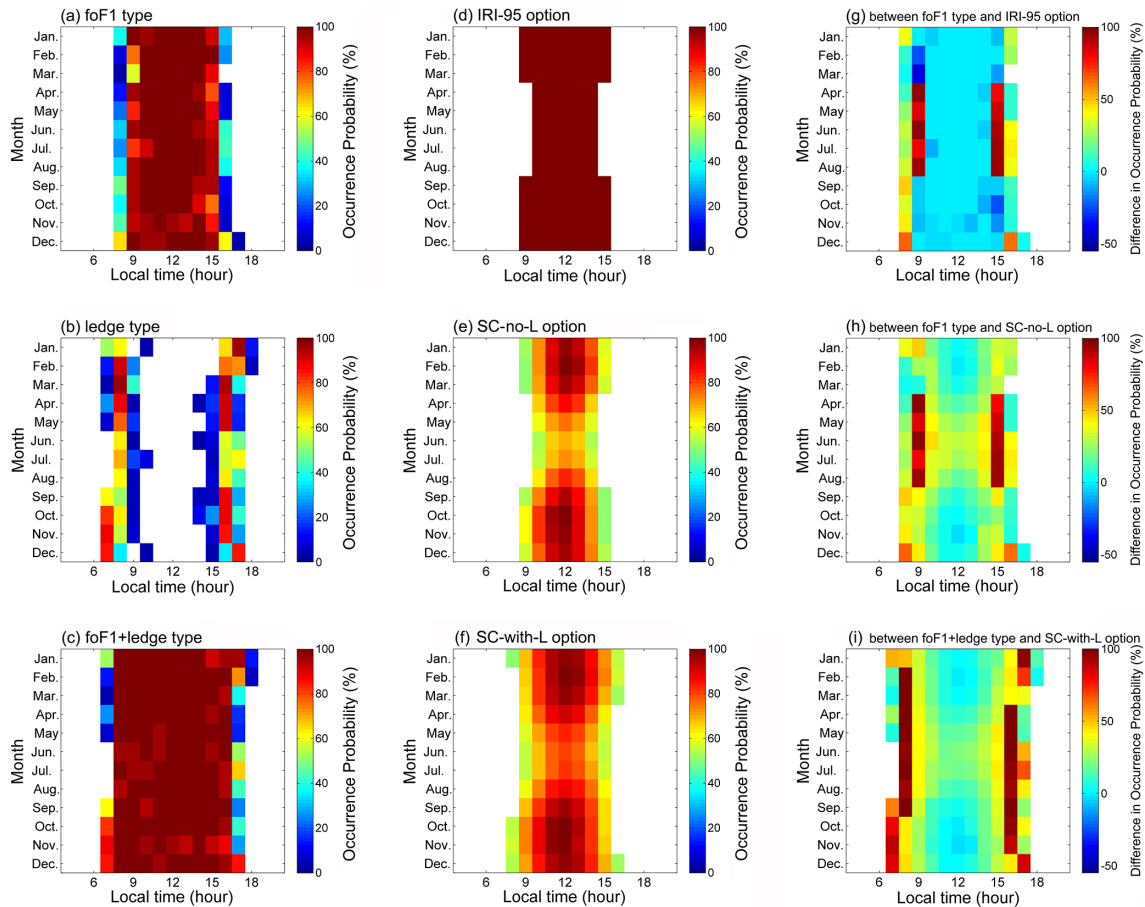
Figure 1. The F1-layer occurrence probabilities for the **(a)** foF1, **(b)** ledge, and **(c)** foF1+ledge types of the Jicamarca digisonde, and for the **(d)** IRI-95, **(e)** SC-no-L, and **(f)** SC-with-L options of IRI-2012 during January–December 1996. The differences in occurrence probabilities **(g)** between foF1 type and IRI-95 option, **(h)** between foF1 type and SC-no-L option, and **(i)** between foF1+ledge type and SC-with-L option are presented.

characteristics of IRI is required. The aim of this paper is to investigate how well the IRI-2012 predicts the F1-layer characteristics at Jicamarca, Peru (12° S, 76.9° W; dip latitude: 1.0° N), during solar minimum. The occurrence probability, NmF1, hmF1, and profile shape parameter (D1) of F1 layer obtained from the observed ionogram are compared with those modeled by IRI-2012. The data period is between January and December 1996. It is noted that the solar cycle 23 started in May 1996 with the monthly smoothed sunspot number of 8.0.

2 Data

In this study, the ionograms were observed by the Jicamarca digisonde (12° S, 76.9° W), located near the geomagnetic equator. The recorded ionograms in 1996 provide the hourly data of F1-layer characteristics during solar minimum. It is noted that the Jicamarca ionograms were downloaded from the Digital Ionogram DataBase (DIDBase), and

the ionograms were manually edited with the SAO Explorer software package (http://ulcar.uml.edu/digisonde.html). The occurrence probability is the number of F1-layer events in a certain hour divided by the number of observed ionograms in this hour for a month. NmF1 is calculated from the critical plasma frequency, foF1, of the F1 layer by NmF1 (el m^{-3}) = $1.24 \times 10^{10} \cdot (fo\text{F1/MHz})^2$. hmF1 and D1 are derived using the true height inversion algorithm NHPC (ftp://umlcar.uml.edu/SoftwareUtilities/NHPC/) (Reinisch and Huang, 2000; Huang and Reinisch, 2001) imbedded in the SAO Explorer software package (Reinisch, 1996; Huang and Reinisch, 2001). D1, a shape parameter, is used to describe the shape of F1-layer profile, obtained from the digisonde observation (Reinisch and Huang, 2000). Moreover, the F1 layer is categorized into two types: (1) foF1 and (2) ledge types (Piggott and Rawer, 1972; Adeniyi and Radicella, 1997). The foF1 type is defined when a well-developed cusp is formed between the E and F2 layers, or a distinct transition point is formed between the end of the F1 layer and the beginning of the F2 layer. For the other type, the F1 layer is not
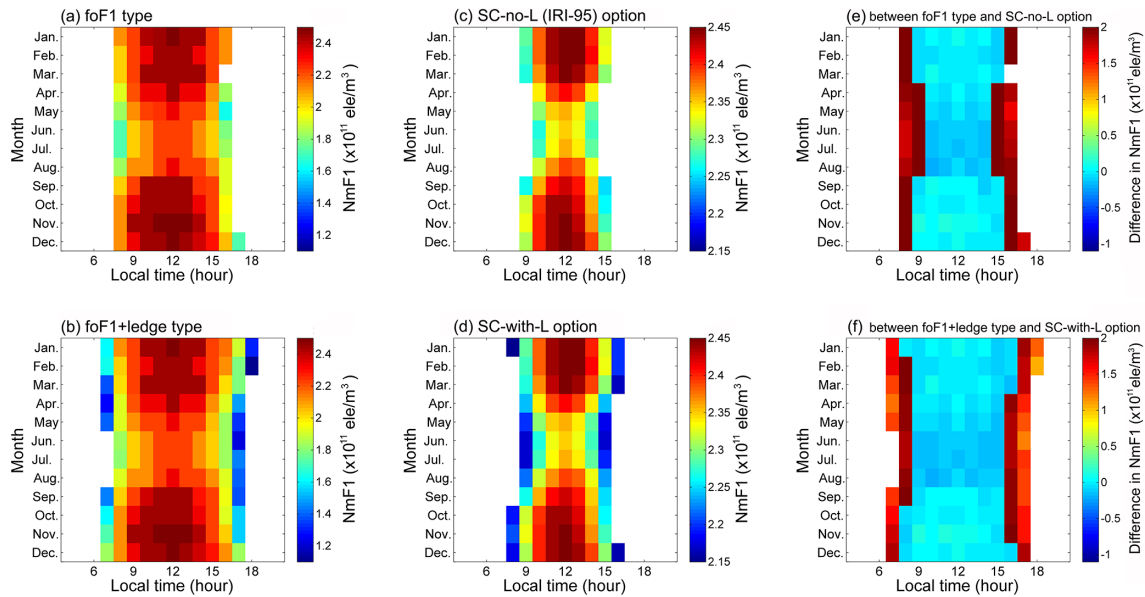
Figure 2. The monthly median *Nm*F1 values for the **(a)** *fo*F1 and **(b)** *fo*F1+ledge types of the Jicamarca digisonde, and for **(c)** SC-no-L and **(d)** SC-with-L options of IRI-2012 during January–December 1996. The differences in *Nm*F1 **(e)** between *fo*F1 type and SC-no-L option, and **(f)** between *fo*F1+ledge type and SC-with-L option are displayed.

fully developed, but a ledge (L-condition) is observed below the F2 layer. To eliminate the effects of geomagnetic disturbances, the data only under geomagnetic quiet conditions ($\Sigma Kp \le 24$) are included in the study. It is noted that the geomagnetic quiet condition is defined as $\Sigma Kp \le 24$, where ΣKp is the sum of the eight 3-hourly Kp indices for a day.

In addition to the observed data, the values of occurrence probability, *Nm*F1, *hm*F1, and C1 modeled by the IRI-2012 are applied in this work. C1 is a shape parameter describing the shape of F1-layer profile of IRI-2012 (Bilitza et al., 1990). Because both C1 and D1 are used to describe the shape of F1-layer profile, C1 of IRI-2012 is compared with D1 of observation. The F1-layer occurrence probability of IRI-2012 has three options: (1) IRI-95 (DuCharme et al., 1973), (2) Scotto-97 no L (SC-no-L), and (3) Scotto-97 with L (SC-with-L) (Scotto et al., 1997). It is noted that "L" in the labels of the last two options represents the L-condition (the ledge type of F1 layer) (Scotto et al., 1997). For the IRI-95 option, an F1 layer (*fo*F1 type) is only assumed to exist when the solar zenith angle (χ) is smaller than or equal to χ_m. χ_m is the maximum solar zenith angle, which is calculated from a function of geomagnetic latitude (λ) and 12-month smoothed sunspot number (R_{12}). The detailed definition of χ_m can be found in DuCharme et al. (1973). The occurrence probability for this option is 0 % (100 %), as $\chi > \chi_m$ ($\chi \le \chi_m$). Regarding the other two options, the occurrence probabilities are calculated from a function of χ, λ, and R_{12}. The definition of the probability function for the SC-no-L and SC-with-L options is described by Scotto et al. (1997). The SC-no-L option gives the occurrence probability of *fo*F1 type,

while the SC-with-L option provides the occurrence probability of *fo*F1+ledge type, which means that both *fo*F1 and ledge types are taken together. For *Nm*F1, only one option is built in the model (DuCharme et al., 1973). Regarding *hm*F1, the value will be affected by the choice of B0 (Bilitza, 1990). Therefore, all three choices of B0 – (1) Gul-1987 (Gulyaeva, 1987), (2) Bil-2000 (Bilitza et al., 2000), and (3) ABT-2009 (Altadill et al., 2008, 2009) – are applied to model *hm*F1. Based on the results of Reinisch and Huang (2000), since IRI-2001, the C1 value has been 2.5 times that of the earlier edition. Furthermore, the observed Ap and F10.7 indices are inputted in the IRI modeling to consider the month-to-month variability. Also, the hourly data of occurrence probability, *Nm*F1, *hm*F1, and C1 under geomagnetic quiet conditions are used in this study.

3 Results and discussions

3.1 Occurrence probability

Figure 1a–c show that the occurrence probabilities of F1 layer, obtained from the Jicamarca ionograms, for the (a) *fo*F1, (b) ledge, and (c) *fo*F1+ledge types during January–December 1996. For the *fo*F1 type (Fig. 1a), the F1 layer appears from 08:00 to 16:00 LT. The occurrence probability does not vary with the seasons. The occurrences are almost 100 % during 10:00–14:00 LT, and exceed 80 % at 09:00 and 15:00 LT. This demonstrates that the F1 layer of *fo*F1 type certainly appears, when χ is smaller than 35°. In Fig. 1b, the ledge type exists generally at 07:00–09:00 LT and

15:00–17:00 LT. The seasonal variation is also not found in the ledge type. In Fig. 1c, it is found that the appearance begins at 07:00 and ends at 17:00 LT, when the *fo*F1 and ledge types are taken together. The occurrences are almost 100 % between 08:00 and 16:00 LT. This indicates that the F1 layer of *fo*F1+ledge type certainly appears, as $\chi < 65°$. For the *fo*F1 type, the occurrence probabilities in this study are similar to the results at low solar activity in Adeniyi (1996) and Adeniyi and Radicella (1997). Adeniyi (1996) and Adeniyi and Radicella (1997) investigated the equatorial F1 layer at Ibadan, Nigeria (7.4° N, 3.9° E; dip latitude: 6.3° S), and Ouagadougou, Burkina Faso (12.4° N, 1.8° W; dip latitude: 5.9° N), respectively. For the ledge type, Adeniyi and Radicella (1997) also reported that, at low solar activity, this type of F1 layer generally appears in the early morning and late afternoon. This result reveals that a ledge-like profile occurs just at the bottom of F2 layer, when an F1 layer starts to be formed in the early morning. And, before the layer vanishes, the *fo*F1-type F1 layer transforms into the ledge type in the late afternoon.

The occurrence probabilities of F1 layer predicted by IRI-2012 are displayed in Fig. 1d–f. The results for the options of IRI-95, SC-no-L, and SC-with-L are presented in Fig. 1d, e, and f, respectively. In Fig. 1d, the occurrence probabilities are 100 %. The appearance is during 09:00–15:00 LT for January–March and September–December, and during 10:00–14:00 LT for April–August. For the SC-no-L and SC-with-L options, the occurrence probability will be outputted by IRI-2012, when its value is greater than or equal to 50 %. In Fig. 1e, the time ranges of appearance for the SC-no-L option are the same as those for the IRI-95 option. The occurrence probability has a diurnal variation with a daily maximum value at 12:00 LT. Moreover, the occurrence probabilities are larger in the summer and equinoctial months but smaller in the winter months. In Fig. 1f, it is found that the diurnal and seasonal variations for the SC-with-L option are similar to those for the SC-no-L option. Nevertheless, the occurrence probability and time range of appearance for the SC-with-L option are slightly larger than those for the SC-no-L option.

Figure 1g–i present the differences in occurrence probabilities between observation and model. In Fig. 1g, the occurrence probabilities of IRI-95 option are compared with those of observation (*fo*F1 type). It is found that the IRI-95 prediction is close to the observation during 10:00–14:00 LT. The positive differences exist at 08:00–09:00 LT and 15:00–16:00 LT, because the time range of appearance is not predicted well by the IRI-95 option. Figure 1h shows the comparison result between observation (*fo*F1 type) and SC-no-L option, while Fig. 1i displays the comparison result between observation (*fo*F1+ledge type) and SC-with-L option. In Fig. 1h and 1i, it is found that the time ranges of appearance of the two options are shorter than those of observation, too. These results suggest that the time range of appearance predicted by IRI-2012 should be extended by at least 1 h
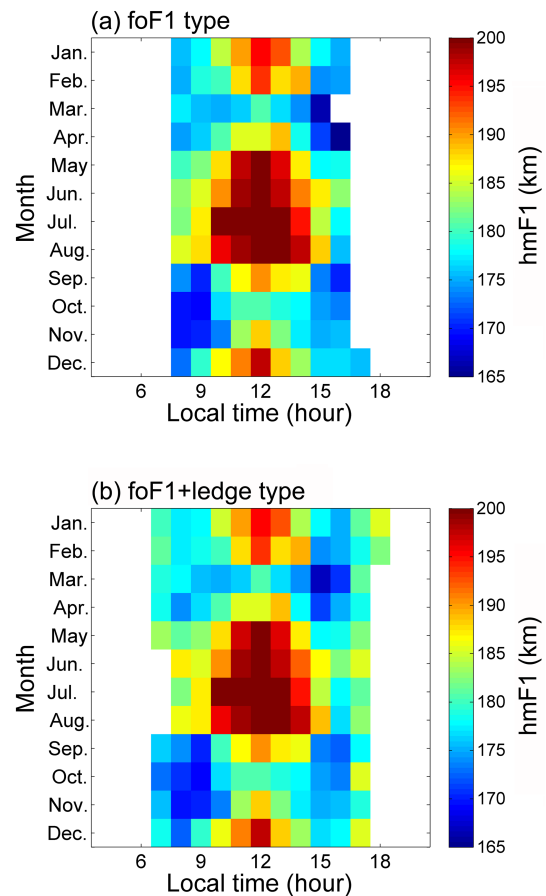

Figure 3. The monthly median *hm*F1 values for the **(a)** *fo*F1 and **(b)** *fo*F1+ledge types of the Jicamarca digisonde during January–December 1996.

in the early morning and late afternoon. Furthermore, both SC-no-L and SC-with-L options significantly underestimate the occurrence probabilities, except during 11:00–13:00 LT of January–March and September–December. These significant differences are mainly because the seasonal variation in occurrence probabilities does not exist in the Jicamarca observation. These results demonstrate that the SC-no-L and SC-with-L options (Scotto et al., 1997) do not predict the occurrence probability of F1 layer well.

3.2 Peak density

The monthly median values of *Nm*F1, observed by the Jicamarca digisonde, for January–December of 1996 are displayed in Fig. 2a–b. In Fig. 2a (*fo*F1 type), there is a diurnal variation in *Nm*F1. The *Nm*F1 values increase from 08:00 LT, have a maximum at 12:00 LT, and then decrease. A seasonal variation exists in *Nm*F1, which has the greater values in the summer and equinoctial months and the smaller values in the winter months. These kinds of diurnal and seasonal variations are also found in the *fo*F1+ledge type (Fig. 2b). These variations suggest that the *Nm*F1 values are dependent on
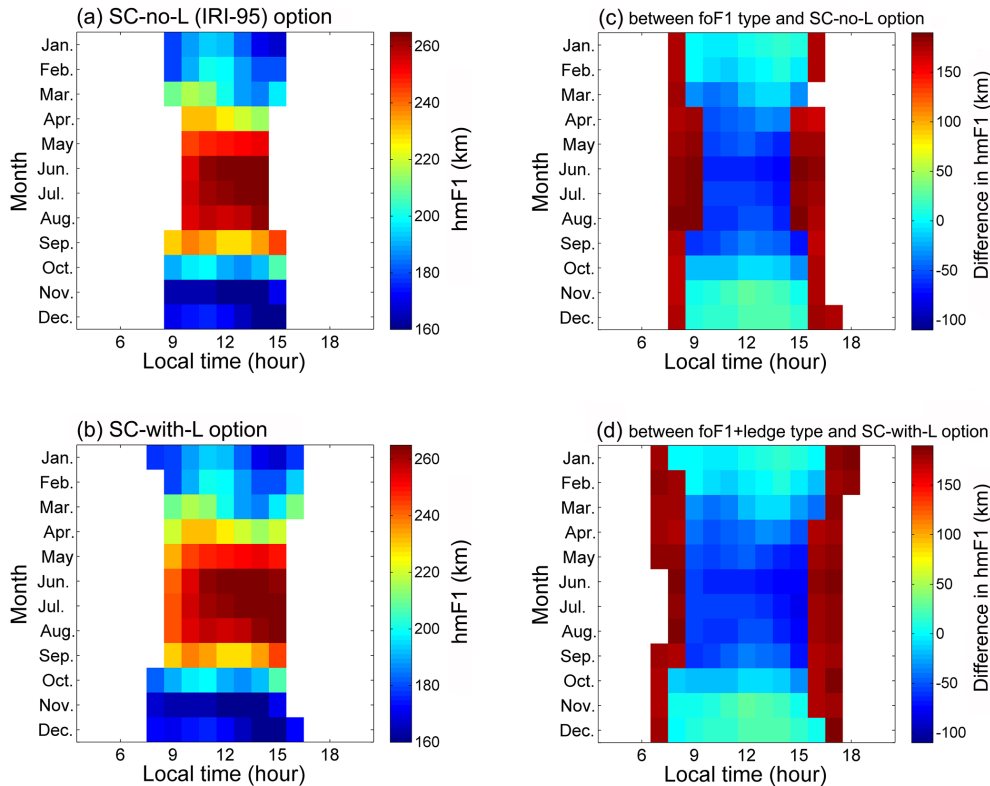
Figure 4. The monthly median *hm*F1 values for **(a)** SC-no-L and **(b)** SC-with-L options, modeled by IRI-2012 with the B0 choice of Gul-1987, during January–December 1996. The differences in *hm*F1 **(c)** between *fo*F1 type and SC-no-L option, and **(d)** between *fo*F1+ledge type and SC-with-L option are displayed.

χ. Here, the correlation coefficient between $\log(Nm\mathrm{F1})$ and $\log[\cos(\chi)]$ for each month is calculated. The correlation coefficient is estimated to be about 0.98 for all 12 months. This further suggests that $Nm\mathrm{F1}$ can be represented by the relation of $Nm\mathrm{F1} = a \cdot \cos^n(\chi)$. The values of a and n are derived to be 2.50×10^{11} ele m^{-3} and 0.33, respectively. The n of 0.33 indicates that the F1 layer is not an idealized Chapman layer, whose n is 0.5 (e.g., Rishbeth and Garriott, 1969). Moreover, according to Rishbeth and Garriott (1969), $Nm\mathrm{F1}$ would vary slowly with χ compared to the peak density of idealized Chapman layer, because the linear loss rate decreases with an increasing height. The values of a and n are close to those in Adeniyi and Radicella (1997), in which a and n were found to be 2.75×10^{11} ele m^{-3} and 0.34. However, there is no seasonal variation in $Nm\mathrm{F1}$ in Adeniyi (1996) and Adeniyi and Radicella (1997).

Figure 2c–d show the monthly median values of $Nm\mathrm{F1}$, provided by IRI-2012, during January–December 1996. Because the $Nm\mathrm{F1}$ variation of IRI-95 option is the same as that of SC-no-L option, the results of only SC-no-L (Fig. 2c) and SC-with-L (Fig. 2d) options are presented. For both options, the diurnal and seasonal variations appear in $Nm\mathrm{F1}$. And these variations generally follow a solar zenith angle variation. The correlation coefficient between $\log(Nm\mathrm{F1})$ and

$\log[\cos(\chi)]$ is also calculated and the value is 1. It is expected that coefficient is 1, because IRI-2012 applies the relation of $Nm\mathrm{F1} = a \cdot \cos^n(\chi)$ to predict $Nm\mathrm{F1}$. Moreover, the values of a and n are derived to be 2.45×10^{11} ele m^{-3} and 0.20, respectively.

In Fig. 2e–f, the differences in $Nm\mathrm{F1}$ between observation and IRI-2012 are calculated. The apparent differences in Fig. 2e are located at 08:00–09:00 LT and 15:00–16:00 LT. In Fig. 2f, the apparent differences exist at 07:00–08:00 LT and 16:00–17:00 LT. These differences are primarily caused by the shorter time ranges of appearance of IRI-2012. Except the apparent differences, IRI-2012 provides a good prediction of $Nm\mathrm{F1}$, because both observed and modeled $Nm\mathrm{F1}$ have the same dependence on χ. Nevertheless, it is necessary to notice that a for IRI-2012 is slightly smaller than for observation, while n for IRI-2012 is greater than for observation.

3.3 Peak height

Figure 3 shows the monthly median values of *hm*F1 for observation during January–December 1996. For the *fo*F1 type (Fig. 3a), the values of *hm*F1 have a diurnal variation. *hm*F1 generally starts to rise at 08:00 LT, has the highest value at 12:00 LT, and then descends. This kind of diurnal variation indicates that *hm*F1 is negatively correlated
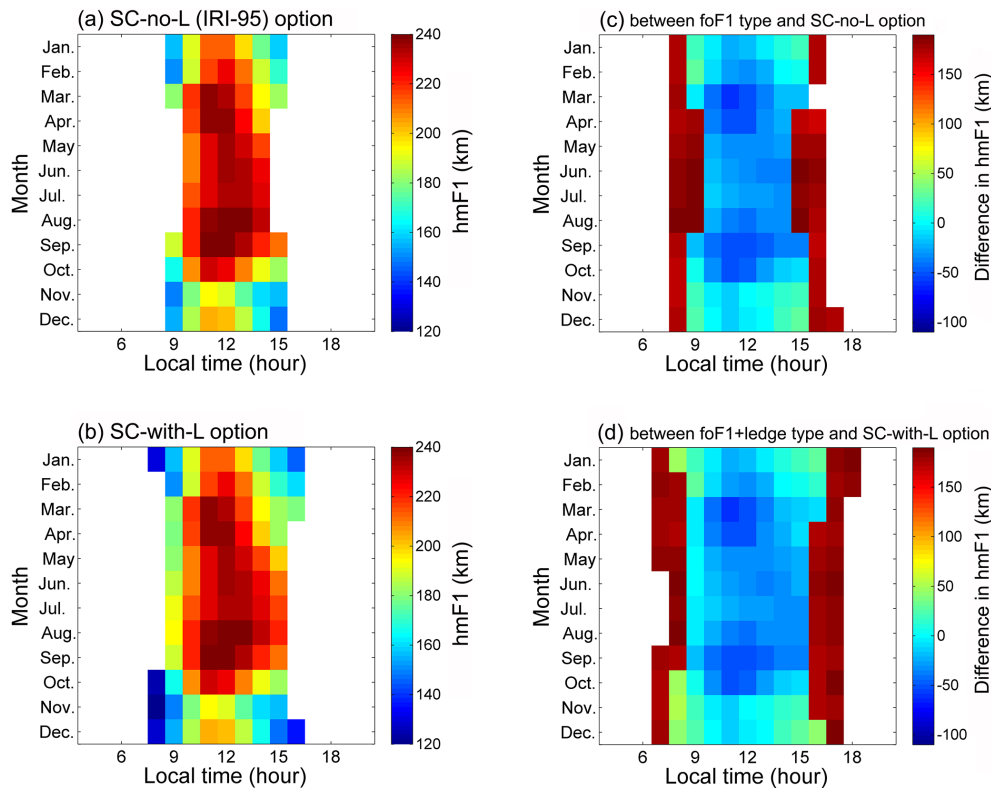
Figure 5. The monthly median *hm*F1 values for **(a)** SC-no-L and **(b)** SC-with-L options, modeled by of IRI-2012 with the B0 choice of Bil-2000, during January–December 1996. The differences in *hm*F1 **(c)** between *fo*F1 type and SC-no-L option, and **(d)** between *fo*F1+ledge type and SC-with-L option are displayed.

with χ. Conversely, the seasonal *hm*F1 variation shows that *hm*F1 is positively correlated with χ, because *hm*F1 is higher (lower) when χ is larger (smaller) in the winter (equinoctial) months. These suggest that the relationship between *hm*F1 and χ can not be used to explain the *hm*F1 variations. Furthermore, these diurnal and seasonal variations would not be caused by the $\boldsymbol{E} \times \boldsymbol{B}$ vertical velocity, because the velocity would not affect the ionosphere below 200 km (Radicella and Adeniyi, 1999; Lee, 2012). In Fig. 3b, the seasonal variation of *fo*F1+ledge type is similar to that of *fo*F1 type. However, the diurnal *hm*F1 variation of *fo*F1+ledge type is partially different to that of *fo*F1 type, when the ledge type is included. *hm*F1 descends from 07:00 to 08:00 LT, and then rises to a maximum height at 12:00 LT. Afterward, *hm*F1 descends again, and then rises from 16:00 to 17:00 LT. Since the ledge-like profile (ledge type) is located just below the F2 layer, the *hm*F1 values are higher in the early morning and late afternoon.

The monthly median values of *hm*F1, modeled by IRI-2012, are presented in Figs. 4a–b, 5a–b, and 6a–b. It is noted that the *hm*F1 variations of only SC-no-L and SC-with-L options are shown in these figures, because the *hm*F1 variation of IRI-95 option is the same as that of SC-no-L option. The *hm*F1 variations for the B0 choice of Gul-1987 are displayed

in Fig. 4a–b. In Fig. 4a (SC-no-L option), the *hm*F1 values are highest and lowest in the winter and summer months, respectively. In the summer and equinoctial months, *hm*F1 starts to rise at 09:00 LT, and has a maximum at 11:00 LT. Afterward, *hm*F1 descends to a minimum at 14:00 LT, and then rises again. For the winter months, *hm*F1 rises gradually during daytime. For the other option (Fig. 4b), the diurnal and seasonal variations of SC-with-L option are similar to those of SC-no-L option. Figure 4c–d show the differences in *hm*F1 between observation and IRI-2012 with B0 choice of Gul-1987. The apparent differences are found at 08:00–09:00 LT and 15:00–16:00 LT in Fig. 4c, and at 07:00–08:00 LT and 16:00–17:00 LT in Fig. 4d, because the time range of appearance for IRI-2012 is shorter than for observation. The significant negative differences are located between March and September. On the other hand, IRI-2012 underestimates *hm*F1 at 12:00–14:00 LT in November and December.

In Fig. 5a–b, the *hm*F1 variations are predicted by the IRI-2012 with B0 choice of Bil-2000. It is found in Fig. 5a that *hm*F1 has a diurnal variation. *hm*F1 rises in morning, has a maximum at 12:00 LT, and then descends in afternoon. For the seasonal variation, the *hm*F1 values are higher in the equinoctial and winter months but lower in the summer months. Furthermore, the diurnal and seasonal variations of
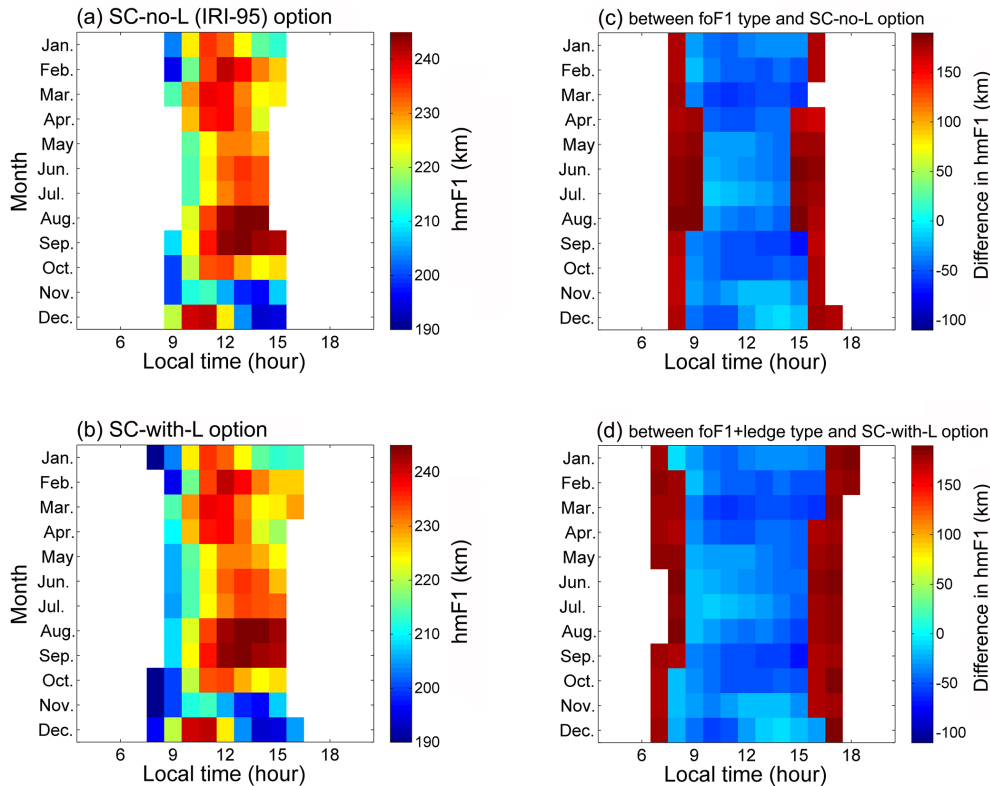
Figure 6. The monthly median hmF1 values for **(a)** SC-no-L and **(b)** SC-with-L options, modeled by IRI-2012 with the B0 choice of ABT-2009, during January–December 1996. The differences in hmF1 **(c)** between foF1 type and SC-no-L option, and **(d)** between foF1+ledge type and SC-with-L option are displayed.

SC-with-L option (Fig. 5b) are similar to those of SC-no-L option (Fig. 5a). For the B0 choice of Bil-2000, the differences in hmF1 between observation and IRI-2012 are displayed in Fig. 5c–d. In addition to the apparent positive differences due to the shorter time range, the positive differences exist at 08:00–09:00 and 14:00–16:00 LT in January, February, November, and December. Moreover, it is found that IRI-2012 with B0 choice of Bil-2000 significantly overestimates hmF1 during February–October.

Figure 6a–b present the hmF1 variations of IRI-2012 with B0 choice of ABT-2009. In Fig. 6a, hmF1 has a diurnal variation with a daily maximum near noon in January, February, and April–September. In March, and October–December, hmF1 starts to rise at 09:00 LT, and has a maximum at 11:00 LT. Afterward, hmF1 descends to a minimum at 14:00 LT, and then rises again. There is no noticeable seasonal variation in hmF1 for this B0 choice. In Fig. 6c–d, the differences in hmF1 between observation and IRI-2012 with B0 choice of ABT-2009 are shown. It is also found that the apparent positive differences due to the shorter time range exist in the early morning and late afternoon. For this B0 choice, IRI-2012 overestimates hmF1 in all 12 months of 1996.

In addition to the differences in hmF1 described above, the seasonal variation in observed hmF1 (Fig. 4) is not similar to those in the IRI-2012 results for all three choices of B0. Overall, IRI-2012 does not give a good prediction of hmF1 at Jicamarca during solar minimum. Moreover, among three B0 choices, the B0 choice of Bil-2000 provides a better representation of hmF1. This is not consistent with the result of Bilitza and Rawer (1990), in which they proposed that the B0 choice of Gul-1987 produced a more accurate value of hmF1.

3.4 Shape parameter

In Fig. 7a–b, the monthly median values of D1, obtained from the digisonde observation, are shown. The D1 values have a diurnal variation in both foF1 and foF1+ledge types. D1 generally starts to increase at 08:00 LT, has a maximum value at 12:00–13:00 LT, and then decreases. Reinisch and Huang (2000) also reported that the diurnal D1 variation at Jicamarca has a systematic behavior going from zero at sunrise, through a maximum at noon, and then to zero again at sunset. Moreover, the D1 values are greater in the summer and winter months, but they are smaller in the equinoctial months. The diurnal and seasonal variations of D1 are qualitatively similar to that of hmF1, except in the early morning and late afternoon.
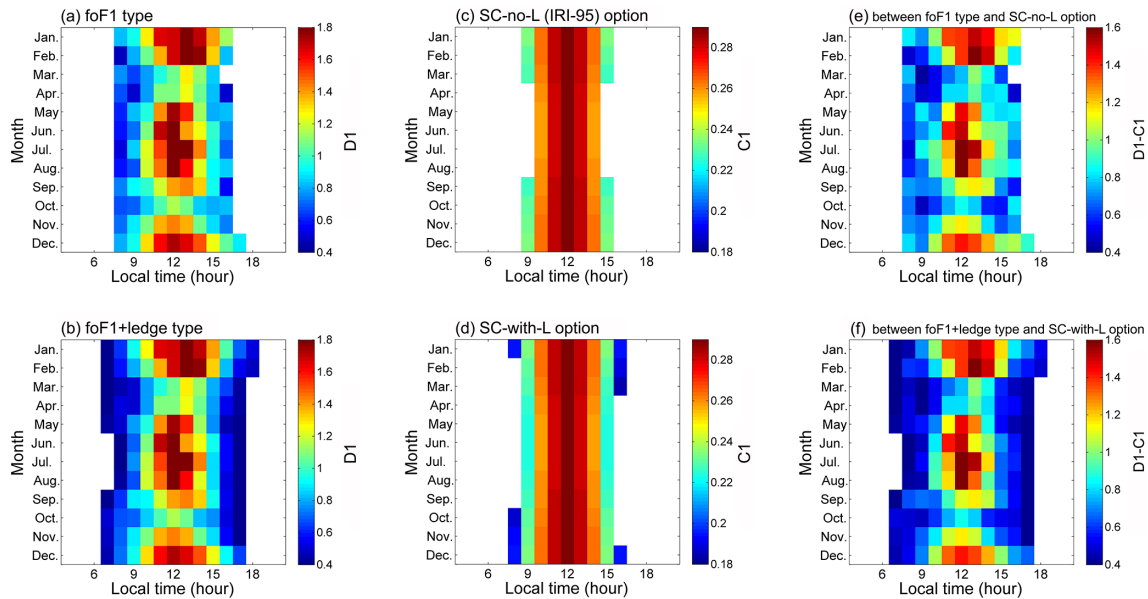
Figure 7. The monthly median D1 values for the **(a)** *fo*F1 and **(b)** *fo*F1+ledge types of the Jicamarca digisonde, and the monthly median C1 values for **(c)** SC-no-L and **(d)** SC-with-L options of IRI-2012 during January–December 1996. The differences between D1 and C1 **(c)** for *fo*F1 type and SC-no-L option, and **(d)** for *fo*F1+ledge type and SC-with-L option are displayed.

Figure 7c–d present the monthly median C1 values of IRI-2012 during January–December 1996. It is noted that the C1 value is applied to calculate the monthly median value, when the corresponding NmF1 is greater than 0. Because the C1 variation of IRI-95 option is the same as that of SC-no-L option, the results of only SC-no-L (Fig. 7c) and SC-with-L (Fig. 7d) options are presented. For both options, the diurnal C1 variation has a daily maximum at 12:00 LT. There is no seasonal variation existing in C1. These variations of C1 are expected, because the C1 values are derived from an Epstein function for a given location and time (Bilitza, 1990).

The differences between D1 and C1 are displayed in Fig. 7e–f. The C1 values are evidently smaller than the D1 values in all 12 months of 1996. The positive differences are greater in the summer and winter months, but they are smaller in the equinoctial months. The difference values greater than 1.5 are found at 12:00 LT in May–August and at 13:00 LT in January–February. And the corresponding ratios of D1 to C1 are greater than 6.0, since the C1 values are 0.28–0.29. Moreover, in the early morning and late afternoon, the difference values are about 0.4, and the corresponding ratio of D1 to C1 is about 3. These results indicate that the D1 values of observation are 3–6 times the C1 values of IRI-2012 at Jicamarca during solar minimum.

4 Conclusion and summary

In order to know how well IRI-2012 predicts the characteristics of F1 layer near the geomagnetic equator during solar minimum, the observed F1-layer characteristics of the Jicamarca digisonde are compared with the modeled results. The period of observed and predicted data is between January and December 1996. It is noted that this period is under the solar minimum between the solar cycle 22 and 23. The characteristics are the occurrence probability, NmF1, hmF1, and D1 (C1) of F1 layer.

For observation, the *fo*F1 type of F1 layer appears during 08:00–16:00 LT, while the *fo*F1+ledge type exists during 07:00–17:00 LT. However, the time ranges of appearance are between 09:00 and 15:00 LT for the IRI-95 and SC-no-L options, and between 10:00 and 16:00 LT for the SC-with-L option. There is need to extend the time range of appearance predicted by IRI-2012. During 10:00–14:00 LT, the IRI-95 option predicts the occurrence probability of *fo*F1 type well, but the SC-no-L option underestimates the probability. The SC-with-L option underestimates the occurrence probability of *fo*F1+ledge type during 08:00–16:00 LT. Furthermore, the seasonal variation in occurrence probability is not found in the observed result, but it is found in the modeled results of the SC-no-L and SC-with-L options.

The diurnal and seasonal variations in NmF1 for the *fo*F1 and *fo*F1+ledge types follow a solar zenith angle variation. NmF1 has a diurnal variation with a daily maximum at 12:00 LT. For the seasonal variation, the NmF1 values are greater in the summer and equinoctial months but smaller in the winter months. NmF1 can be represented by the relation of NmF1 $= a \cdot \cos^n(\chi)$. In both the diurnal and seasonal variations, the observed and predicted NmF1 values are close to each other. IRI-2012 provides a good prediction of NmF1.

For the foF1 type, hmF1 begins to ascend at 08:00 LT, has a maximum height at noon, and then falls. This kind of diurnal variation is qualitatively similar to the diurnal hmF1 variations for the B0 choices of Bil-2000 and ABT-2009, except in March and October–December for ABT-2009. However, for all three B0 choices, IRI-2012 generally overestimates the hmF1 values. For the foF1+ledge type, the diurnal hmF1 variations of observation are different to those of IRI-2012 for all three B0 choices. For the seasonal variation, the observed hmF1 values are highest and lowest in the winter and equinoctial months, respectively. The seasonal variation of observation is not similar to those of the model. Overall, IRI-2012 does not predict the hmF1 values well.

The diurnal variation of D1 has a daily maximum at noon for the foF1 and foF1+ledge types. Although this kind of diurnal variation can be found in C1 of IRI-2012, the values of C1 are obviously smaller than those of D1. The D1 values are greater in the summer and winter months, but they are smaller in the equinoctial months. However, there is no seasonal variation in C1. Moreover, the D1 values are 3–6 times the C1 values.

References

Abdu, M. A., Batista, I. S., Reinisch, B. W., and Carrasco, A. J.: Equatorial F-layer heights, evening prereversal electric field, and night E-layer density in the American sector: IRI validation with observation, Adv. Space Res., 34, 1953–1965, 2004.

Adeniyi, J. O.: Equatorial F1 characteristics and the international reference ionosphere model, Radio Sci., 31, 893–897, 1996.

Adeniyi, J. O. and Adimula, I. A.: Comparing the F2 layer model of IRI with observations at Ibadan, Adv. Space Res., 15, 141–144, 1995.

Adeniyi, J. O. and Radicella, S. M.: Electron density and height at F1 region minimum gradient at low solar activity for an equatorial station, Radio Sci., 32, 1867–1874, 1997.

Adeniyi, J. O. and Radicella, S. M.: Diurnal variation of ionospheric profile parameters B0 and B1 for an equatorial station at low solar activity, J. Atmos. Solar-Terr. Phys., 60, 381–385, 1998a.

Adeniyi, J. O. and Radicella, S. M.: Variation of bottomside profile parameters B0 and B1 at high solar activity for an equatorial station, J. Atmos. Solar-Terr. Phys., 60, 1123–1127, 1998b.

Adeniyi, J. O., Bilitza, D., Radicella, S. M., and Willoughby, A. A.: Equatorial F2-peak parameters in the IRI model, Adv. Space Res., 31, 507–512, 2003.

Altadill, D., Arrazola, D., Blanch, E., and Buresova, D.: Solar activity variations of ionosonde measurements and modeling results, Adv. Space Res., 42, 610–616, 2008.

Altadill, D., Torta, J. M., and Blanch, E.: Proposal of new models of the bottom-side B0 and B1 parameters for IRI, Adv. Space Res., 43, 1825–1834, 2009.

Batista, I. S. and Abdu, M. A.: Ionospheric variability at Brazilian low and equatorial latitudes: comparison between observations and IRI model, Adv. Space Res., 34, 1894–1900, 2004.

Bilitza, D.: International Reference Ionosphere: Recent development, Radio Sci., 21, 343–346, 1986.

Bilitza, D. (Ed.): International Reference Ionosphere 1990, NSSDC 90-22, Greenbelt, Maryland, 1990.

Bilitza, D.: International Reference Ionosphere 2000, Radio Sci., 36, 261–275, 2001.

Bilitza, D. and Rawer, K.: New options for IRI electron density in the middle ionosphere, Adv. Space Res., 10, 7–16, 1990.

Bilitza, D. and Reinisch, B. W.: International Reference Ionosphere 2007: Improvements and new parameters, Adv. Space Res., 42, 599–609, doi:10.1016/j.asr.2007.07.048, 2008.

Bilitza, D., Radicella, S., Reinisch, B. W., Adeniyi, J., Mosert, M., Zhang, S., and Obrou, O.: New B0 and B1 models for IRI, Adv. Space Res., 25, 89–95, 2000.

DuCharme, E. D., Petrie, L. E., and Eyfrig, R.: A method for predicting the F1 layer critical frequency based on the Zurich smoothed sunspot number, Radio Sci., 10, 837–839, 1973.

Gulyaeva, T. L.: Progress in ionospheric informatics based on electron density profile analysis of ionogram, Adv. Space Res., 7, 39–48, 1987.

Huang, X. and Reinisch, B. W.: Vertical electron content from ionograms in real time, Radio Sci., 36, 335–342, 2001.

Lee, C. C.: Examination of the absence of noontime bite-out in equatorial total electron content, J. Geophys. Res., 117, A09303, doi:10.1029/2012JA017909, 2012.

Lee, C. C. and Reinisch, B. W.: Quiet-condition hmF2, NmF2, and B0 variations at Jicamarca and comparison with IRI-2001during solar maximum, J. Atmos. Solar-Terr. Phys., 68, 2138–2146, 2006.

Lee, C. C. and Reinisch, B. W.:Variations in equatorial F2-layer parameters and comparison with IRI-2007 during a deep solar minimum, J. Atmos. Solar-Terr. Phys., 74, 217–223, 2012.

Lee, C. C., Reinisch, B. W., Su, S.-Y., and Chen, W. S.: Quiet-time variations of F2-layer parameters at Jicamarca and comparison with IRI-2001 during solar minimum, J. Atmos. Solar-Terr. Phys., 78, 184–192, 2008.

Obrou, O. K., Bilitza, D., Adeniyi, J. O., and Radicella, S. M.: Equatorial F2 layer peak height and correlation with vertical ion drift and M(3000)F2, Adv. Space Res., 31, 513–520, 2003.

Piggott, W. R. and Rawer, K.: U.R.S.I. Handbook of Ionogram Interpretation and Reduction, Rep. UAG-23A, World Data Center A for Solar Terr. Phys., Boulder, Colorado, 1972.

Radicella, S. M. and Adeniyi, J. O.: Equatrorial ionospheric electron density below the F2 peak, Radio Sci., 24, 1153–1163, 1999.

Rawer, K., Bilitza, D., and Ramakrishnan, S.: International Reference Ionosphere, International Union of Radio Science (URSI), Brussels, Belgium, 1978.

Reinisch, B. W.: Modern Ionosondes, in: Modern Radio Science, edited by: Kohl, H., Ruester, R., and Schlegel, K., European Geophysical Society, Katlenburg-Lindau, Germany, 440–458, 1996.

Reinisch, B. W. and Huang, X.: Finding better B0 and B1 parameters for the IRI F2 profile function, Adv. Space Res., 22, 741–747, 1998.

Reinisch, B. W. and Huang, X.: Redefining the IRI F1 layer profile, Adv. Space Res., 25, 81–88, 2000.

Rishbeth, H. and Garriott, O. K.: Introduction of ionospheric physics, Academic Press, New York and London, 1969.

Scotto, C., Mosert de Gonzáles, M., Radicella, S. M., and Zolesi, B.: On the prediction of F1 ledge occurrence and critical frequency, Adv. Space Res., 20, 1773–1775, 1997.